Journal of Power Sources 243 (2013) 24–28

Contents lists available at SciVerse ScienceDirect

Journal of Power Sources

journal homepage: www.elsevier.com/locate/jpowsour

Short communication

$BaZr_{0.9}Yb_{0.1}O_{3-\delta}$-modified bi-electrode supported solid oxide fuel cells with enhanced coking and sulfur tolerance

Kevin S. Blinn, Meilin Liu*

School of Materials Science and Engineering, Georgia Institute of Technology, Atlanta, GA 30342, USA

HIGHLIGHTS

- Coking and sulfur poisoning tolerance for a BSC-type Ni SOFC anode is improved.
- A $BaZr_{0.9}Yb_{0.1}O_{3-\delta}$ surface modification is used to achieve this improvement.
- The modified anode's performance is correlated with morphology and phase properties.

ARTICLE INFO

Article history:
Received 8 February 2013
Received in revised form
22 May 2013
Accepted 25 May 2013
Available online 8 June 2013

Keywords:
Solid oxide fuel cell
Anode
Coking
Sulfur poisoning
Jet fuel
Raman spectroscopy

ABSTRACT

Among different designs of solid oxide fuel cells (SOFCs), bi-electrode supported cells (BSC) offer great prospects for superior specific power density due to low weight and volume. This BSC architecture is used as a platform for an anode surface modification study to increase the anode's coking and sulfur poisoning resistance when operating under common hydrocarbon-containing fuels. Here we report a Ni anode modified by $BaZr_{0.9}Yb_{0.1}O_{3-\delta}$ particles that demonstrates stable performance in CH_4 (without coking) and decreased sulfur poisoning. The anode was fabricated by infiltrating Ni precursor into a porous YSZ scaffold in combination with small amounts of Ba, Zr, and Yb nitrates. The electrochemical performances of the modified anodes were compared with blank Ni anodes infiltrated in the same manner. In addition, the structure, morphology, and phase composition of the anodes were studied using X-ray diffraction, microscopy, and Raman spectroscopy.

1. Introduction

Solid oxide fuel cells (SOFCs) represent one of the cleanest, most efficient, and most versatile electrical energy production systems [1]. Unlike most other types of fuel cells, by virtue of their high operating temperatures, SOFCs may employ catalyst materials that give them the ability to utilize not only hydrogen (H_2) but also hydrocarbon fuels. Thus, SOFCs can potentially give access to higher efficiency and lower emissions when using familiar fossil fuels as well as renewable bio-fuels with only H_2O and CO_2 gas emissions [2–4], the latter of which can be sequestered and stored for further use [5]. Furthermore, novel cell designs such as the bi-electrode supported cell (BSC) developed by the SOFC team at NASA Glenn Research Center [6,7] can be used to increase specific power density and open up the possibility for SOFCs to be implemented in aeronautical applications such as auxiliary power units (APUs) in commercial aircraft and unmanned aerial vehicles (UAVs).

The basic BSC architecture consists of two porous YSZ scaffolds prepared by a freeze-casting technique acting as electrode supports that are connected by a dense layer of YSZ as the solid electrolyte. The electrode scaffolds have thin layers of functional materials that are ideally porous, interconnected, and firmly adhered to the YSZ in order to make them electrochemically active. Since the freeze-casting scaffold fabrication process itself does not easily accommodate multiple phases like cermets, these layers are applied using solution infiltration techniques afterward. The porosity of the scaffolds is functionally graded in order to maximize gas flow and diffusion as well as triple phase boundaries (TPBs) for electrochemical activity. The shrinking size and directionality of the pores towards the electrolyte also create capillary forces that pull infiltrated solution towards the electrolyte and assist in maximizing the coverage of the scaffold by the electrode layer. The BSC architecture has a potential for high specific power density (e.g. >1 kW kg^{-1}) by

* Corresponding author. Tel.: +1 404 894.6114.
E-mail addresses: kevin.blinn@gatech.edu (K.S. Blinn), meilin.liu@mse.gatech.edu (M. Liu).

0378-7753/$ – see front matter © 2013 Elsevier B.V. All rights reserved.
http://dx.doi.org/10.1016/j.jpowsour.2013.05.177

addressing the main technical obstacles facing SOFC stacks. For example, since current collection occurs throughout most of the cell, due to the infiltrated electrodes, the interconnect used for cell stacks need not be very thick.

The current BSC specifications include state-of-the-art electrode materials such as $La_{0.6}Sr_{0.4}Co_{0.2}Fe_{0.8}O_{3-\delta}$ (LSCF) cathodes and Ni-based anodes. Unfortunately, the Ni anodes limit the types of fuels with which the cell may operate. Ni is very prone to carbon deposition ("coking") on its surface [3,8,9]. Therefore, supplying a Ni-based anode in a BSC with hydrocarbons would likely result in very aggressive coking and quick anode degradation. In addition, such anodes are susceptible to deactivation by sulfur contaminants in the fuel stream. Some fuels, even when desulfurized by the most modern techniques, still contain 10 ppm of sulfur species or more [10], and a more conventional fuel treatment will produce a fuel with sulfur content that has only been reduced to the 100 ppm range [11]. These levels of sulfur content in the fuel stream would be sufficient to cripple a Ni anode cell's performance within a short time [12]. While much work needs to be done before SOFCs that can operate under a fuel stream containing both hydrocarbons and sulfur can be produced, the work reported here represents a step in that direction.

Indeed, solving degradation problems caused by coking and sulfur poisoning on SOFC anodes in the presence of common hydrocarbon fuels is a key to unlocking the SOFC's potential as a mainstream power source. Candidate anode materials and structures other than the traditional porous Ni–YSZ composites have been considered by SOFC researchers to this end, such as doped $SrTiO_3$, double perovskites, and $BaZr_{0.1}Ce_{0.7}Y_{0.1}Yb_{0.1}O_{3-\delta}$ (BZCYYb) [13–19]. In particular, BZCYYb has promising applications for coking resistance and sulfur poisoning tolerance. In previous work, a Ni–BZCYYb composite anode showed virtually no performance loss when operated in C_3H_8 fuel and H_2 fuel with up to 50 ppm H_2S content [18]. Unfortunately, all of these materials face one or more of the following problems in their applicability to practical fuel cell systems: physical, chemical, and thermal incompatibilities with state-of-the-art YSZ electrolyte, relatively high cost, and lower overall catalytic performance. On the other hand, efforts have been made to improve the degradation tolerance of more conventional Ni–YSZ by modifying the surface of Ni with nanostructured "islands" of BaO [3] and Y-doped $BaZrO_3$ coatings [20].

In order to make BSC-type SOFCs truly fuel-flexible and an ideal power system, the issues of anode tolerance to coking and sulfur poisoning need to be addressed in a manner that does not hinder the cell's performance in other ways. One possible route for overcoming these problems is modification of the infiltrated Ni anode layers with oxide nanoparticles, which would essentially create an active cermet anode layer. Results of previous research have demonstrated that oxides containing Ba and Yb with an affinity for water can play a role in staving off coking and sulfur poisoning respectively [3,18,20] while improving anode oxidation performance. Therefore, a nominal $BaZr_{0.9}Yb_{0.1}O_{3-\delta}$ (BZYb) composition was chosen for the oxide nanoparticles in the current work due to the incorporation of the Ba and Yb elements as well as the relative compatibility of $BaZrO_3$-based oxides with Ni–YSZ electrodes [20]. To date, the use of Yb-doped barium zirconates has been generally limited to proton-conducting electrolytes [19,21,22]; thus, this work's application of BZYb in particular is a novel one.

2. Experimental details

First, circular YSZ BSC tri-layer scaffolds with a ~40-mm diameter were prepared by a freeze-casting very similar to one described elsewhere [6,7]. The electrode layers each had a thickness of ~1 mm, while the dense electrolyte had a thickness of ~50 μm. The anodes were prepared by alternating infiltrations from a stock solution of 100 g $Ni(NO_3)_2$ (~8 M concentration) in 20 g methanol and modification solution (0.03 M total metal ion concentration) on one face of the YSZ scaffold. The BZYb solution itself was prepared using the appropriate metal precursors ($Ba(NO_3)_2$, $Zr(NO_3)_2O$, and $Yb(NO)_3$ hydrates), citric acid, EDTA, and ammonium hydroxide. The stock solution was diluted with deionized water to achieve the 0.03 M concentration. A sample of the stock solution was evaporated, calcined to 1000 °C, and characterized by Raman spectroscopy (Renishaw RM1000, 514 nm excitation) and XRD (Phillips X'Pert, Cu Kα edge) to confirm the formation of the BZYb phase.

For infiltration, the solutions were applied drop-wise to one face of the scaffold until visibly saturated. Before applying the infiltrant to one face, the opposite face of the scaffold was masked with a viscous solution of polypropylene carbonate (QPAC40 by Empower Materials, 10 wt.%) in acetone in order to prevent cross-contamination between the two electrodes. The scaffold was then heated up to 450 °C on a hot plate over ~2 h, held at temperature for 15 min, and then cooled down. Over the course of the heating, the acetone evaporated and the polypropylene carbonate decomposed into water vapor and CO_2, so virtually no undesirable residue was left behind by the mask. Ni and modification solutions were alternately infiltrated 6 times each in this manner in order to establish an active electrode layer with a thickness of several μm. Ni-only cells were also infiltrated to be used as control samples. All sample slabs were heated to 1000 °C for 2 h to complete the conversion of the anode layer to its constituent oxides. Next, a heavily concentrated La–Sr–Co–Fe nitrate solution with appropriate stoichiometry to eventually form the perovskite LSCF was infiltrated on the opposite face from the anode and heated to 450 °C in order to create the cell's cathode. This step was also repeated a total of 6 times. The completed cell slabs were heated again to 900 °C to complete the conversion of the cathode layer to LSCF perovskite. All heat treatment was performed in air.

Cell performance and anode stability were tested in H_2, CH_4, and H_2S-containing fuel gases by voltammetry. For testing in H_2 and CH_4 fuels, the full 40-mm infiltrated BSC scaffolds were used as test cells. Silver mesh was used as current collector for both electrodes and was attached using gold paste. A fine platinum wire voltage lead was also attached near the outer part of the electrode to assist with current collection. Cells were mounted in a clamshell furnace and heated to 800 °C. A 75% H_2/25% N_2 gas flow (400 sccm) was fed to the anode for 1 h in order to reduce the Ni, after which the stability and performance testing was performed on the cell using the same H_2 gas mixture or a CH_4 flow (75 sccm). Fuel was fed through a room-temperature water bubbler before reaching the cell to give the gas a 3% H_2O content. A 1000 sccm air flow was used to flood the cathode side with oxygen. For testing in H_2S-containing fuel, 1-cm button cells cut by laser from the 40-mm scaffolds were used. For the button cells, current collection was achieved using Ag paste and wire. The cells were tested at 700 °C with a wet 40 sccm H_2 gas flow containing 20 ppm H_2S fed to the anode. In order to achieve this gas, an 8 sccm flow of H_2 containing 100 ppm H_2S was combined with a 32 sccm flow of H_2 that was passed through a room-temperature water bubbler. The cathode was exposed to ambient air as the oxygen source.

Cell microstructure was examined using scanning electron microscopy (SEM, JEOL JSM) before and after operation, and Raman spectroscopy was used to assess cell degradation following operation.

3. Results and discussion

Fig. 1 shows the XRD pattern and Raman spectrum obtained from BZYb powder calcined at 1000 °C from the modification

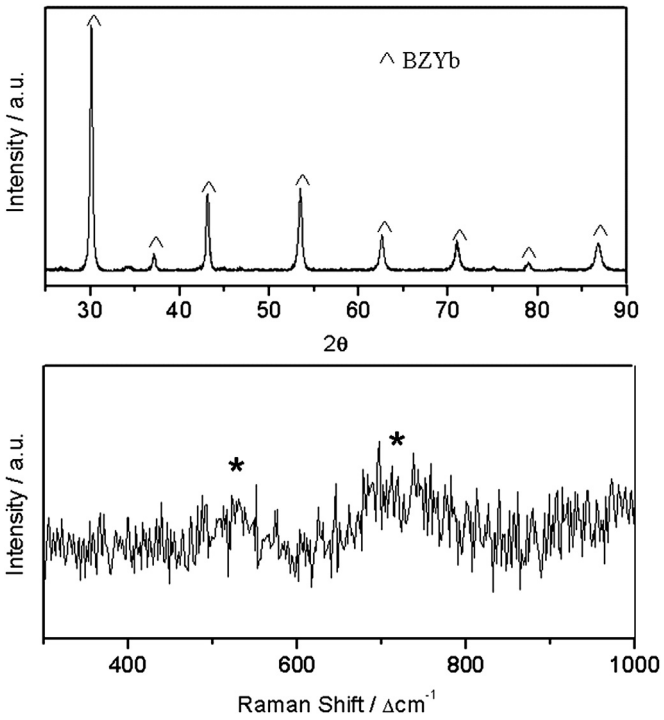

Fig. 1. XRD pattern (top) and Raman spectrum (bottom) collected from BZYb powder calcined from solution.

solution. The XRD pattern matches the one found by Ahmed et al. in their study of $BaZr_{0.9}Yb_{0.1}O_{3-\delta}$ and confirms that the material's overall structure matches the space group $Pm\bar{3}m$ [22]. Other very small peaks seen in the pattern, such as the one at 34°, possibly indicate a minor $BaCO_3$ impurity in the powder. For the Raman spectrum, though no Raman lattice phonon modes are predicted by group theory for this material, the doping-induced defects likely produce the broad features that are visible in the spectrum. These results confirm that the desired phase was largely achieved from the modification solution.

BZYb-infiltrated cells exhibit stable operation in low-order hydrocarbon fuel at high temperatures. The performance of these cells is also superior. Fig. 2a and b presents a comparison of the performances in H_2 and CH_4 fuels between 40-mm cells with unmodified and BZYb-modified anodes. The modified cells show nearly 100% improvement in both cases. The BZYb-modified cell also show relatively good stability over 2 days of testing when operated in wet CH_4 at 800 °C compared to the blank cell, which displays a sharp performance decrease after less than 1 h of testing (Fig. 2c). After this performance loss, the blank cell was able to return to an OCV close to its original value (~1.08) upon cutting off the current, indicating that the performance loss was related to anode coking rather than leakage or a sudden shorting of the cell. In addition, the blank cell was able to operate in CH_4 somewhat normally long enough to collect an *IV* curve, which typically only took 5–10 min.

While fuel utilization is not necessarily optimized for this study since only single cells are used, to serve as another performance comparison metric, utilization, or the percentage of fuel apparently oxidized at the anode, may be calculated with the following equation:

$$U_{fuel} = 2.24{*}10^4{*}\frac{jA}{0.97{*}nF\dot{V}}$$

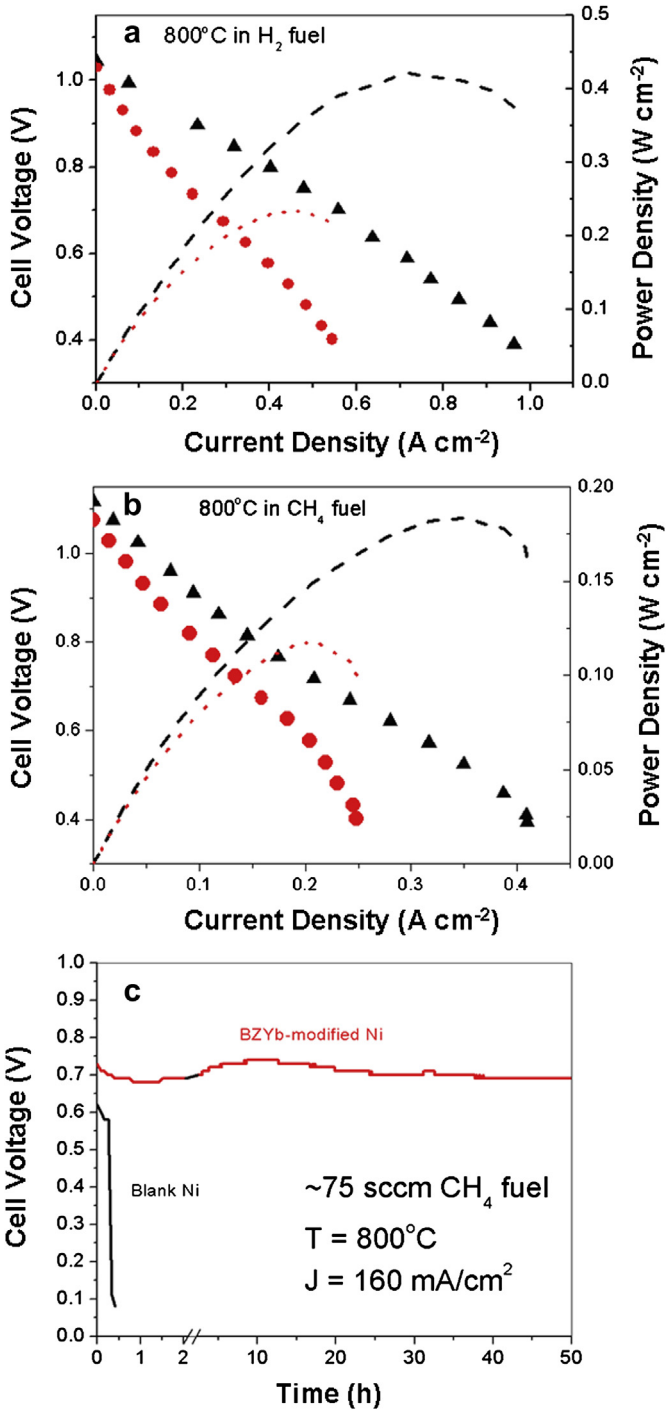

Fig. 2. Current–voltage and power density curves for unmodified (red/circle trace) and BZYb-modified (black/triangle trace) cells operating in (a) wet H_2 and (b) CH_4 fuels at 800 °C, along with (c) performance stability over time of unmodified and BZYb-modified 40-mm cells operating in wet CH_4 fuel at 800 °C. Active area was approximately 12.5 cm^2. (For interpretation of the references to colour in this figure legend, the reader is referred to the web version of this article.)

A is the active electrode area of the cell in cm^2, $\dot{V}$ is the flow rate of the fuel in $cm^3\ s^{-1}$, *F* is Faraday's constant, *j* is current density expressed in A cm^{-2}, and *n* is the number of charges required to completely oxidize a molecule of fuel (2 for H_2 and 8 for CH_4). The factor $2.24 * 10^4$ is the volume of one mole of gas, which is assumed to have ideal behavior, at room temperature in cm^3, and the 0.97 factor corresponds to 3% H_2O that is bubbled into in the fuel stream.

This equation also carries the assumptions that the fuel gas pressure is near atmospheric level and the oxidant flow does not limit the cell reaction. Since the cathode is flooded with air in this experimental setup, the latter is a fair assumption. Finally, in the case of CH_4 oxidation, a direct oxidation assumption is not too far from reality as the eventual products are water and oxides of carbon, although this assumption does not take into account the possibility of internal reforming. Fuel utilizations calculated at peak power density for the BZYb-modified large cell operating at 800 °C are ~23% and ~11% for H_2 and CH_4, respectively, which are quite high for the size of the single cells being used here. The CH_4 fuel utilization value, in particular, is relatively high compared to those values calculated from data found in contemporary literature for similar Ni–YSZ systems operated at 800 °C, which are anywhere between <1% and 6% [23,24].

After electrochemical testing, the large cells' anodes were characterized by SEM. Fig. 3a shows a low-magnification SEM image of a typical anode in order to demonstrate the porous structure of the BSC scaffold. Fig. 3b–e displays high-magnification SEM images collected from the surface of the scaffold walls of each type of anode after operation in CH_4. The unmodified anode's structure degrades considerably as a result of aggressive coking; the porous Ni anode layer disintegrates into relatively isolated granules. In addition, the cylindrical shape that can be seen in Fig. 3b is likely fibrous carbon. In contrast, for the BZYb-modified anode, the porous Ni layer is left intact. Spheroid-shaped particles decorate the top of the anode layer; these particles are likely BZYb. Raman spectroscopy was used to probe for the presence of carbon on the anodes after CH_4 operation. Fig. 3f shows Raman spectra obtained from each anode. Most of the features observed in both spectra are assigned to YSZ (e.g. 620 cm^{-1}) as well as fluorescence due to impurities with the material [25]. In the unmodified anode, sharp D-band and G-band carbon peaks respectively centered near 1350 cm^{-1} and 1600 cm^{-1} superimposed over the broad fluorescence band centered at 1610 cm^{-1} clearly indicate carbon deposition [26,27]. The intensity of the G-band is only slightly higher than that of the D-band, indicating a mix of amorphous and relatively ordered carbon [27]. This character likely corresponds to the mix of structures seen in Fig. 3b and c. On the other hand, these peaks are not visible in the spectrum from the modified sample. Meanwhile, the shoulder near 700 cm^{-1}, while seemingly present in both spectra, protrudes more for the modified sample spectrum, indicating the presence of the same weak band at 720 cm^{-1} seen in the Raman spectrum in Fig. 1. This feature therefore can be assigned to the BZYb modification.

Sulfur tolerance tests were performed on the BZYb-modified anode using button-sized cells. Fig. 4 displays the results of a typical poisoning and recovery test with 20 ppm H_2S in the gas feed. Since these cells had much smaller active areas than the larger

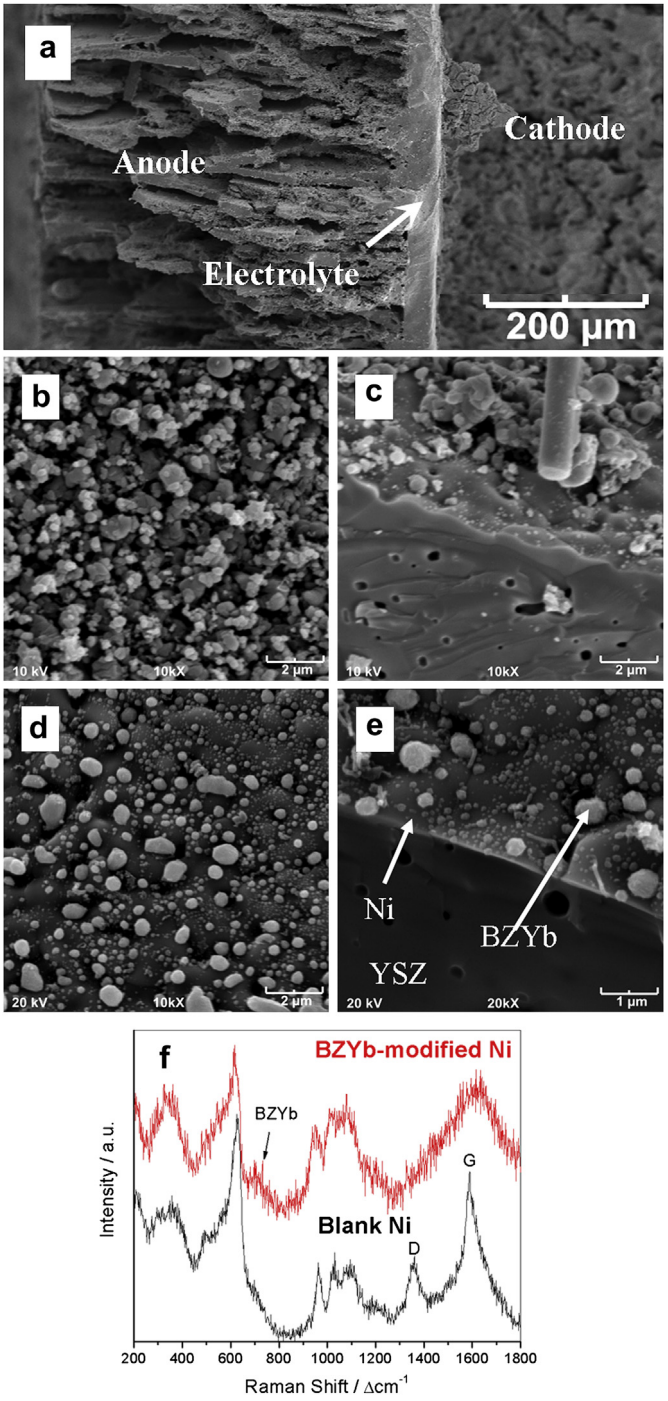

Fig. 3. SEM images of (a) a lower magnification micrograph of a typical infiltrated BSC scaffold, the top surface of (b, c) unmodified Ni anode, and (d, e) BZYb-modified Ni anode following operation of cells in CH_4 at 800 °C, along with (f) Raman spectra collected from unmodified and BZYb-modified cells following operation in CH_4 fuel at 800 °C.

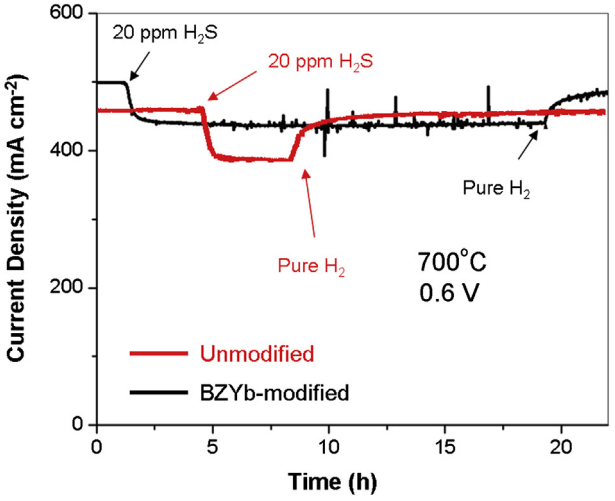

Fig. 4. Operation stability over time of cells containing an unmodified Ni anode (red trace) and a BZYb-modified Ni anode (black trace) in H_2 with and without 20 ppm H_2S content. Active area was approximately 0.18 cm^2. (For interpretation of the references to colour in this figure legend, the reader is referred to the web version of this article.)

cells, they had better apparent current density at 700 °C than the larger cells did at 800 °C; thus, direct comparisons between them should be made with caution [7]. While the difference in performance between the two cells represented in Fig. 4 appear to be somewhat small, for the BZYb-modified button cell, the performance only drops by 10% in 20 ppm H_2S, which is a better result compared with the button cell with a blank Ni anode, which has a performance drop of 20%. In addition, both types of cells fully recover their performance after removal of the H_2S from the fuel stream. Therefore, the BZYb modification at least provides some suppression in the sulfur poisoning while not leading to any permanent poisoning as a trade-off.

The actual mechanism by which coking was prevented and sulfur poisoning is suppressed remains somewhat vague. As was the case in previous studies involving modification of SOFC anodes with Ba-containing oxides [3,18,20,26], the tolerance is likely water-remediated. Internal reforming, which is known to occur when CH_4 is used as a fuel in SOFCs at high temperatures, might also be improved by the presence of BZYb. The initial results given by the BZYb modification are promising, so it may prove to be a good benchmark material for further studies towards truly unraveling what role these oxides play in tolerance mechanisms.

4. Conclusion

This work has demonstrated that a BZYb oxide can be successfully infiltrated into the Ni–YSZ anode of a BSC-structured cell, providing coking and sulfur poisoning resistance. The BZYb modification also conveys considerable performance improvement to cell and allows for better fuel utilization. Therefore, this material system could provide a good avenue for ongoing and future anode studies. For example, how the anodes perform under more realistic conditions, such as fuel streams containing both hydrocarbons and H_2S, is a more complex issue that is part of ongoing research. If improved internal reforming is part of the coking tolerance mechanism, whether or not H_2S affects this internal reforming is an issue that should be addressed. For other future work, the detailed effects of composition, morphology, and microstructure of BZYb-modified anodes could be systematically examined to optimize performance, coking resistance, and sulfur poisoning tolerance. Longer exposure and operation tests should be performed in order to assess long-term stability. In addition, the connection between intrinsic material properties (i.e. water adsorption capability, mass transport), architecture, and tolerance characteristics of such modifications might be investigated in future work in order to find the optimal conditions for cell performance and anode stability.

Acknowledgment

This work was supported in by the NASA Graduate Student Researchers Program under Grant Number NNX10AL43H. The authors would like to thank Dr. Serene C. Farmer and Mr. John Setlock at the NASA Glenn Research Center for kindly providing the scaffolds and advice on infiltration techniques used in this work.

References

[1] N.Q. Minh, Solid State Ionics 174 (2004) 271–277.
[2] M. Liu, M.E. Lynch, K. Blinn, F. Alamgir, Y. Choi, Mater. Today 14 (2011) 534–546.
[3] L. Yang, Y. Choi, W. Qin, H. Chen, K. Blinn, M. Liu, P. Liu, J. Bai, T.A. Tyson, M. Liu, Nat. Commun. 2 (2011) 357.
[4] S.C. Singhal, Solid State Ionics 152 (2002) 405–410.
[5] S. Vivanpatarakij, N. Laosiripojana, W. Kiatkittipong, A. Arpornwichanop, A. Soottitantawat, S. Assabumrungrat, Chem. Eng. J. 147 (2009) 336–341.
[6] T.L. Cable, S.W. Sofie, J. Power Sources 174 (2007) 221–227.
[7] T.L. Cable, J.A. Setlock, S.C. Farmer, A.J. Eckel, Int. J. Appl. Ceram. Technol. 8 (2011) 1–12.
[8] A. Atkinson, S. Barnett, R.J. Gorte, J.T.S. Irvine, A.J. McEvoy, M. Mogensen, S.C. Singhal, J. Vohs, Nat. Mater. 3 (2004) 17–27.
[9] Y. Lin, Z. Zhan, J. Liu, S.A. Barnett, Solid State Ionics 176 (2005) 1827–1835.
[10] Y. Wang, J. Latz, R. Dahl, J. Pasel, R. Peters, Fuel Process. Technol. 90 (2009) 458–464.
[11] J. Latz, R. Peters, J. Pasel, L. Datsevich, A. Jess, Chem. Eng. Sci. 64 (2008) 288–293.
[12] M. Flytzani-Stephanopoulos, M. Sakbodin, Z. Wang, Science 312 (2006) 1508–1510.
[13] J.-S. Kim, V.V. Nair, J.M. Vohs, R.J. Gorte, Scr. Mater. 65 (2011) 90–95.
[14] O.A. Marina, N.L. Canfield, J.W. Stevenson, Solid State Ionics 149 (2002) 21–28.
[15] J.C. Ruiz-Morales, J. Canales-Vazquez, C. Savaniu, D. Marrero-Lopez, W. Zhou, J.T.S. Irvine, Nature 439 (2006) 568–571.
[16] Q. Ma, F. Tietz, A. Leonide, E. Ivers-Tiffee, J. Power Sources 196 (2011) 7308–7312.
[17] Y.H. Huang, R.I. Dass, Z.L. Xing, J.B. Goodenough, Science 312 (2006) 254–257.
[18] L. Yang, S. Wang, K. Blinn, M. Liu, Z. Liu, Z. Cheng, M. Liu, Science 326 (2009) 126–129.
[19] C. Chen, M. Liu, Y. Bai, L. Yang, E. Xie, M. Liu, Electrochem. Commun. 13 (2011) 615–618.
[20] M.F. Liu, Y.M. Choi, L. Yang, K. Blinn, W. Qin, P. Liu, M.L. Liu, Nano Energy 1 (2012) 448–455.
[21] N. Osman, A.M. Jani, I.A. Talib, Ionics 12 (2006) 379–384.
[22] I. Ahmed, S.-G. Eriksson, E. Ahlberg, C.S. Knee, H. Gotlind, L.-G. Johansson, M. Karlsson, A. Matic, L. Borjesson, Solid State Ionics 178 (2007) 515–520.
[23] A. Singh, J. Hill, J. Power Sources 214 (2012) 185–194.
[24] J. Myung, H.J. Ko, J.-J. Lee, S.-H. Hyun, Int. J. Electrochem. Sci. 6 (2011) 1617–1629.
[25] M.A. Laguna-Bercero, V.M. Orera, Int. J. Hydrogen Energy 36 (2011) 13051–13058.
[26] K.S. Blinn, H.W. Abernathy, X. Li, M.F. Liu, M. Liu, Energy Environ. Sci. 5 (2012) 7913–7917.
[27] A. Cuesta, P. Dhamelincourt, J. Laureyns, A. Martínez-Alonso, J.M.D. Tascón, Carbon 32 (1994) 1523–1532.